

Impact of an Active Sgr A* on the Synthesis of Water and Organic Molecules Throughout the Milky Way

Chang Liu,¹ Xian Chen,^{1,2} and Fujun Du³

¹*Department of Astronomy, School of Physics, Peking University, Beijing 100871, China*

²*Kavli Institute for Astronomy and Astrophysics, Beijing 100871, China*

³*Purple Mountain Observatory, Chinese Academy of Sciences, Nanjing 210008, China*

Abstract

Sgr A*, the supermassive black hole (SMBH) in our Galaxy, is dormant today, but it should have gone through multiple gas-accretion episodes in the past to grow to its current mass of $4 \times 10^6 M_{\odot}$. Each episode temporarily ignites the SMBH and turns the Galactic Center into an active galactic nucleus (AGN). Recently, we showed that the AGN could produce large amount of hard X-rays that can penetrate the dense interstellar medium in the Galactic plane. Here we further study the impact of the X-rays on the molecular chemistry in our Galaxy. We use a chemical reaction network to simulate the evolution of several molecular species including H₂O, CH₃OH, and H₂CO, both in the gas phase and on the surface of dust grains. We find that the X-ray irradiation could significantly enhance the abundances of these species. The effect is the most significant in those young, high-density molecular clouds, and could be prominent at a Galactic distance of 8 kpc or smaller. The imprint in the chemical abundance is visible even several million years after the AGN turns off. The potential impact on the origin and evolution of organic and prebiotic molecules in the Milky Way deserves further investigation.

Keywords: astrochemistry — Galaxy: abundances — ISM: abundances — ISM: molecules — X-rays: ISM

1. Introduction

Supermassive black holes (SMBHs) are ubiquitous in the centers of massive galaxies (Kormendy & Ho 2013). In theory, a SMBH grows to its current mass mainly through multiple episodes of gas accretion (Volonteri 2010). In each accretion phase a significant fraction of the gravitational energy of the gas is released in the form of radiation, and the galaxy center consequently becomes an active galactic nucleus (AGN, Soltan 1982). Analysis of the luminosity function of bright AGNs indicates that the accretion episodes may add up to about (1 – 10)% of the lifetime of a galaxy (Hopkins & Hernquist 2009; Shankar et al. 2009). The SMBHs in the mass range of ($10^6 - 10^7$) M_{\odot} on average are more active in the sense that they become AGNs every $10^7 - 10^8$ years while each active phase only lasts $10^5 - 10^6$ years (Hopkins et al. 2006).

The center of the Milky Way (MW) also harbors a SMBH. It coincides with the bright radio source

Sagittarius A* (Sgr A*) and the mass is estimated to be $4 \times 10^6 M_{\odot}$ (Genzel et al. 2010). This black hole (BH) is dormant today, but in the past it should have been active according to the close relationship between SMBH growth and AGN activity (Mezger et al. 1996). One interesting discovery in the last decade is that Sgr A* may be an AGN just several million years (Myrs) ago. This picture is supported by a series of findings, including the Fermi bubble (Su et al. 2010), the bright emission of H α lines in the Magellanic Stream (Bland-Hawthorn et al. 2013), and the young stellar disk around Sgr A* which is reminiscent of a relic accretion disk (see Chen & Amaro-Seoane 2015, for a review). The peak luminosity of that recent AGN is unclear and the current estimations fall in a broad range of (3 – 100)% of the Eddington limit $L_{\text{Edd}} \simeq 5 \times 10^{44} \text{ erg s}^{-1}$ (Nayakshin & Cuadra 2005; Bland-Hawthorn et al. 2013). Such a high level of activity is not completely unexpected given the aforementioned frequent activity of low-mass BHs.

Not many works have explored the impact of an active Sgr A* on the habitability of the MW. Early studies identified X-ray and cosmic rays as a potential threat to

lives but they lacked a theoretical framework to quantify the damage (Clarke 1981; Lavolette 1987; Gonzalez 2005). Amaro-Seoane & Chen (2019, Paper I) adopted an empirical AGN spectral energy distribution (SED) and calculated the extinction of light in the Galactic plane. They found that hard X-rays (> 2 keV) could reach Earth unattenuated and the corresponding flux is comparable to an X-class solar flare. They also suspected that the high X-ray irradiation may have a noticeable impact on the molecular chemistry in the MW. Other works neglected the attenuation of light and focused on the evaporation of planet atmosphere during the AGN irradiation (Balbi & Tombesi 2017; Chen et al. 2018; Forbes & Loeb 2018; Wisłocka et al. 2019). Their general conclusion is that mass loss is significant only within a distance of 1 kpc from Sgr A*. More recently, Lingam et al. (2019) explored possible beneficial effects associated with the AGN irradiation, such as a prebiotic synthesis of the building blocks of biomolecule and a powering of photosynthesis on free-floating planets. Based on the estimation of the UV flux, they reached a similar conclusion that only in the central kpc of the MW are these effects important.

In this work, we continue our early study of the impact of an active Sgr A* on the habitability of the MW. We focus on hard X-ray irradiation because, unlike optical and UV, hard X-ray photons are not attenuated by the gas in the Galactic plane and hence could reach large distances (see Paper I). It is known, from studying the molecular clouds in star-forming regions, that hard X-rays could enhance the abundance of organic molecules such as CN, C₂H, HC₃N (Krolik & Kallman 1983; Lepp & Dalgarno 1996). The main reason is that X-rays, by ionizing atoms and molecules, create energetic electrons (Shull & van Steenberg 1985; Maloney et al. 1996), which, by further interacting with the atoms and molecules, produce reactive ions and radicals (Herbst & Klemperer 1973; Herbst & van Dishoeck 2009). Ions and radicals, compared to neutral species, react more quickly to produce complex molecules (Herbst & van Dishoeck 2009; Wakelam et al. 2010).

Because of the close relationship between X-ray irradiation and the synthesis of organic molecules, we expect an imprint of the recent active Sgr A* in the abundance of complex molecules in the MW. This is a reasonable expectation also because abnormal molecular abundance has been detected in extragalaxies with AGNs (Usero et al. 2004). For example, the column density of H₂O and other biogenic and organic species such as HCN, HCO⁺, and CH₃OH are particularly high in extragalactic AGNs (González-Alfonso et al. 2010; Davies et al. 2012; Imanishi & Nakanishi 2014;

Takano et al. 2014; Harada et al. 2018). Given the current capability of detecting these species, we pay special attention to them in this work.

This paper is organized as follows. In §2 we calculate the X-ray irradiation spectra at different distances from Sgr A*, and we also specify our X-ray chemical model, especially the processes associated with H₂O, CH₃OH, and H₂CO. In §3 we describe our simulation of the molecular chemistry induced by X-ray irradiation. The results are presented in §4, where we show the dependence of the abundance of different molecules on the distance, column density, and lifetime of a molecular cloud. We discuss the caveats of our current model in §5 and finally summarize our conclusions in §6.

2. X-ray Chemistry in Molecular Clouds

2.1. X-ray Source

To calculate the X-ray flux during the AGN phase of Sgr A*, we use a numerical model which is described in detail in Liu et al. (2016). This model computes the SED of an accretion disk based on three parameters, the Eddington ratio defined as $\eta := L/L_{\text{Edd}}$ where L is the bolometric luminosity of the disk, the X-ray spectral index α , and the magnetic parameter β which characterizes the relative importance between the sum of the gas and radiative pressure and the magnetic pressure. In this model, hard X-rays are produced by a hot corona screening the disk. The solid curves in Figure 1 show the output SED as a function of the Eddington ratio. In the calculation we assume that $\alpha = 0.1$, $\beta = 100$, and the BH mass is $4 \times 10^6 M_{\odot}$. We find that when $\eta \gtrsim 1$, the total luminosity above 2 keV is more or less constant, about 10^{43} erg s⁻¹. This result from numerical simulation is consistent with our analytical estimation in Paper I. When $\eta \lesssim 0.5$, we find that the luminosity of hard X-ray falls linearly with decreasing Eddington ratio.

Soft photons are subject to extinction as they propagate in the Galactic plane. To quantify it, we adopt the empirical density profile of the atomic hydrogen $\rho_{\text{H}}(R)$ and molecular hydrogen $\rho_{\text{H}_2}(R)$ in the MW (McMillan 2017), and we use the software `Xspec`¹ to calculate the extinction. Since most molecular clouds are inside the Galactic plane, we only consider the horizontal (in-plane) gas distribution. The corresponding column density at a Galactic distance of R is

$$\Sigma(R) = \int_0^R [\rho_{\text{H}}(x) + \rho_{\text{H}_2}(x)] dx. \quad (1)$$

¹ <https://heasarc.gsfc.nasa.gov/xanadu/xspec/>

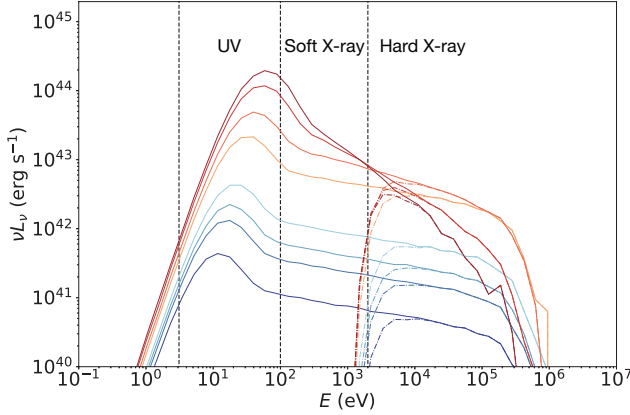


Figure 1. The SED of Sgr A* if its bolometric luminosity is (3.0, 2.0, 1.0, 0.5, 0.1, 0.05, 0.03, 0.01) times the Eddington rate. The solid curves show the unabsorbed SEDs and the dot-dashed ones account for the extinction at a Galactic distance of 8 kpc.

The residual SEDs at $R = 8$ kpc, for example, are shown in Figure 1 as the dot-dashed curves. We can see that the optical and UV radiation is completely absorbed. For this reason, in our chemistry model we focus on the effects induced by X-rays.

2.2. X-ray Ionization

It is mainly through ionization that X-ray irradiation could affect the chemistry inside a molecular cloud (Maloney et al. 1996). Other effects, such as Coulomb heating, are less important in an environment where the ionization fraction x_e is relatively low. In our model we consider two types of ionization.

Primary ionization, also known as the direct photoionization, is caused by an X-ray photon striking an atom (e.g. Latif et al. 2015). The primary ionization rate for a given species i can be calculated with

$$\zeta_p^i = \int_{E_{min}}^{E_{max}} \frac{F(E)}{E} e^{-\tau(E)} \sigma^i(E) dE, \quad (2)$$

where $F(E)$ is the monochromatic X-ray flux incident on the surface of a molecular cloud, $\sigma^i(E)$ is the photoionization cross section given a photon energy of E (Verner et al. 1996), τ is the optical depth defined as

$$\tau(E) = \sum_{i=H,He} N_i \sigma^i(E), \quad (3)$$

and N_i is the column density of a species. In calculating the optical depth, we have taken into account the fact that H (mostly in molecular hydrogen) and He contribute to most of the opacity.

The photoelectrons released in primary ionization could further collide with other atoms and cause secondary ionization (Maloney et al. 1996; Stäuber et al.

2005). In principle, the secondary ionization rate can be calculated with

$$\zeta_{sec}^i = \int_{E_{min}}^{E_{max}} \frac{F(E)}{E} e^{-\tau(E)} N_{sec}(E, x_e) \sigma^i(E) dE, \quad (4)$$

where $N_{sec}(E, x_e)$ is the number of secondary ionization events produced by each photoelectron in average. If the energy of the photoelectron is E , this number can be calculated with

$$N_{sec}(E, x_e) = \frac{\eta_{ion}(x_e)E - E_{th}}{W(E)}, \quad (5)$$

where η_{ion} is the fraction of the photoelectron's energy which goes into secondary ionization, E_{th} is the ionization threshold of an atom, and W is the mean energy needed to produce an ion-electron pair. In practice, we simplify the calculation by adopting the ionization rates presented in Shull & van Steenberg (1985). These rates are derived from a Monte Carlo simulation of the secondary ionization of H and He atoms over a wide range of electron fraction ($0.0001 < x_e < 1$) and photoelectron energy (from 100 eV to several keV).

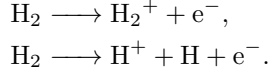
Although we have two types of ionization in our model, the secondary ionization rate predominates. For example, if we consider a typical value of $x_e \leq 1\%$ for a cold ($T \sim 10$ K) molecular cloud, approximately 40% of the energy of primary photoelectrons goes into secondary ionization. Since the ground state of neutral H has a ionization threshold $E_{th} = 13.6$ eV, using $\eta_{ion} = 40\%$ and $W(E) = E_{th}$, we find that for a typical primary photoelectron with $E = 1$ keV, the number for secondary ionization events it will cause is $N_{sec}(E, x_e) \approx 30$.

For H_2 , H and He, we consider both primary and secondary ionization. For heavy elements (C, N, O, etc.) and molecules (CO, CO_2 , etc.), we consider only the secondary ionization for simplicity. We assume that the ionizing electrons are mainly from the three most abundant neutral species, i.e., H_2 , H and He. Then the ionization rate of heavy elements and molecules can be derived from

$$\zeta^m = \frac{\sigma_{ei,m}(E)}{\sigma_{ei,H}(E)} \zeta_{sec}^H, \quad (6)$$

where $\sigma_{ei}(E)$ is the electron-impact cross section at energy E (Maloney et al. 1996; Ádámkóvics et al. 2011). We note that heavy elements are usually bound in molecules, but the current derivation of $\sigma_{ei}(E)$ assumes that the cross section is unaffected by the molecular binding energy. Moreover, we notice that the ratio of the cross sections, which appears in the last equation, is insensitive to E (Maloney et al. 1996). For this reason, we use the cross sections at $E = 50$ eV, which is the typical energy of the secondary electrons.

For completeness, we also consider the destruction of H_2 and several other molecules caused by photoionization. For example, photoionization of H_2 can have two possible outcomes, pure ionization and dissociation, which can be expressed as



We take the branching ratio suggested by Krolik & Kallman (1983), that the fraction of pure ionization is approximately 80% and that for dissociation is 20%. For other atomic and molecular reactants, we adopt the same products from the chemical database `osu_01_2007`², as well as the corresponding branching ratios for cosmic-ray ionization and dissociation.

2.3. Grain Processes

The surface of a dust particle (grain) is an important place for the synthesis of complex molecules. A grain accretes from the surrounding gas many molecular species to its surface, where these molecules can interact more frequently and the chemical reactions such as hydrogenation can proceed more efficiently. Since we are interested in the synthesis of H_2O , CH_3OH , and H_2CO (see §1), we include in our model the surface reactions containing the species made of H, C, N, O. Table 1 shows the relevant reactions, which are selected from the network presented in Hasegawa et al. (1992).

Table 1. Surface reaction network.

Reactant 1	Reactant 2	Product 1	Product 2
H	H	H_2	
H	C	CH	
H	N	NH	
H	O	OH	
H	CH	CH_2	
H	NH	NH_2	
H	OH	H_2O	
H	C_2	C_2H	
H	CN	HCN	
H	CO	HOC	
H	CO	HCO	
H	NO	HNO	
H	O_2	O_2H	

Table 1 *continued*

Table 1 (*continued*)

Reactant 1	Reactant 2	Product 1	Product 2
H	N_2	N_2H	
H	CH_2	CH_3	
H	NH_2	NH_3	
H	C_2H	C_2H_2	
H	HOC	CHOH	
H	HCO	H_2CO	
H	O_2H	H_2O_2	
H	O_3	O_2	OH
H	C_2N	HCCN	
H	N_2H	N_2H_2	
H	CH_3	CH_4	
H	H_2CO	HCO	H_2
H	CHOH	CH_2OH	
H	H_2O_2	H_2O	OH
H	N_2H_2	N_2H	H_2
H	HCCN	CH_2CN	
H	C_2H_2	C_2H_3	
H	C_2H_3	C_2H_4	
H	CH_2OH	CH_3OH	
H	CH_2CN	CH_3CN	
H	C_2H_4	C_2H_5	
H	C_2H_5	C_2H_6	
H_2	OH	H_2O	H
C	C	C_2	
C	N	CN	
C	O	CO	
C	CH	C_2H	
C	NH	HNC	
C	OH	HOC	
C	OH	CO	H
C	CN	C_2N	
C	NO	OCN	
C	O_2	CO	O
C	CH_2	C_2H_2	
C	NH_2	HNC	H
C	OCN	CO	CN
C	CH_3	C_2H_3	
N	N	N_2	
N	O	NO	
N	CH	HCN	
N	NH	N_2H	
N	C_2	C_2N	

Table 1 *continued*

² https://faculty.virginia.edu/.archived/ericherb/research_files/osu_01_2007

Table 1 (*continued*)

Reactant 1	Reactant 2	Product 1	Product 2
N	NH ₂	N ₂ H ₂	
O	O	O ₂	
O	CH	HCO	
O	NH	HNO	
O	OH	O ₂ H	
O	CN	OCN	
O	O ₂	O ₃	
O	CO	CO ₂	
O	HCO	CO ₂	H
O	CH ₂	H ₂ CO	
O	CH ₃	CH ₂ OH	
CH	CH	C ₂ H ₂	
CH	OH	CHOH	
CH	HNO	NO	CH ₂
CH	CH ₃	C ₂ H ₄	
OH	OH	H ₂ O ₂	
OH	CH ₂	CH ₂ OH	

We calculate the accretion rate of molecules onto dust grains following the method developed in Hasegawa et al. (1992). We consider accretion, via weak van der Waals forces (physisorption), onto “classic” dust grains, which have a fixed radius $r_d = 1000$ Å, a density of $\rho = 3$ g/cm³, and $N_s = 10^6$ sites for adsorption (the number of molecules that can be absorbed to and held on a dust grain). The dust temperature T_d is assumed to be the same as the gas temperature $T \sim 10$ K. For the gas-to-dust ratio in mass, we adopt the standard value of 100. We assume that the velocities of the gas species obey Maxwell distribution. For any species that strikes a dust grain, a sticking probability of 1 is assumed.

For the desorption of molecules, we consider three channels, namely, thermal desorption, cosmic-ray desorption, and photo-desorption. (i) Given the adsorption energy E_D and dust temperature T_d , the thermal evaporation rate can be calculated with $R_{\text{evap}} \propto E_D^{1/2} \exp[-E_D/kT_d]$ (Hasegawa et al. 1992), where k is the Boltzmann constant. The value of E_D for each species is from Allen & Robinson (1977) and Hasegawa & Herbst (1993). We note that although thermal evaporation is common, the rate is negligible for any species heavier than He because of the low temperature in our molecular clouds. (ii) The cosmic-ray induced desorption rates are calculated as in (Hasegawa & Herbst 1993). Every time a cosmic-ray particle strikes a dust grain, the dust temperature is assumed to rise to 70 K immediately and then drop via

thermal desorption. (iii) Photo-desorption can be induced by either UV or X-ray photons. For UV-induced desorption, we assume a rate of 10^{-3} molecule per grain per incident UV photon for any species in our grain-surface network (also see Visser et al. 2011). Since UV-induced desorption depends strongly on the visual extinction, which is a function of the optical depths of a molecular cloud, we will study in §4.3 the dependence of the rate on the column density of the molecular cloud. The X-ray desorption processes are more complex (see Jiménez-Escobar et al. 2018 for a brief review) and not as well understood both in theory and in experiment. However, X-ray photons are more penetrative than UV photons, so that the interaction happens deeper inside the bulk of a grain and hence does not as often lead to desorption. Therefore, the X-ray desorption is less significant compared to UV photo-desorption and we neglect it in our model.

3. Simulation

We solve the evolution of the chemical network using the public package KROME³ (Grassi et al. 2014). The initial conditions are as follows. Our molecular cloud has a gas temperature of $T = 10$ K and a density of $n_H = 2 \times 10^4$ cm⁻³. The initial abundances of elements are taken from the EA2 model in Wakelam & Herbst (2008), which is based on the high-metal environment observed in the diffuse cloud of ζ Ophiuchi and is modified based on recent observations of cold cores. For the species at different depths of a molecular cloud, we assume that they follow the same initial abundances.

In our model, even when there is no X-ray irradiation, we include a low level of ionization caused by cosmic rays. The corresponding ionization rate is $\zeta = 1.3 \times 10^{-7}$ s⁻¹ per hydrogen atom (Wakelam & Herbst 2008). We also include a generic UV background according to Draine (1978). Given the UV flux, we calculate the photo-ionization and photo-desorption rates following the scheme presented in §2.

To simulate the impact of the AGN, we turn on X-ray chemistry in the network according to the method described in §2.2 and §2.3. The X-ray SED is calculated assuming a fiducial Eddington ratio of $\eta = 1$ and the flux decreases with with the Galactic distance as R^{-2} . The extinction of X-ray photons by the Galactic plane is taken into account following §2.1. The duration of the X-ray irradiation is set to 10^6 years, to be consistent with the empirical evidence (§1). After that, we turn off the X-ray and let the network evolve for another 10^7

³ <http://krome.package.org/>

years. By the end of the simulation, we investigate the abundance of the molecular species at different Galactic distances to look for possible imprints of an AGN. In our fiducial model we use $R = 4$ kpc (§4.1). We also run simulations using $R = (1, 2, 8)$ kpc for comparison (§4.2).

We notice that as the system evolves, the chemical abundance is no longer uniformly distributed inside a molecular cloud because the extinction of UV and X-ray radiation varies at different depth of the cloud. The depth h can be characterized by the column density of hydrogen, N_{H} , which is related to h as $N_{\text{H}} = n_{\text{H}} h$. Therefore, to understand the abundance of molecular species at different depth in a cloud, we run simulations using different N_{H} . Given the value of N_{H} , the extinction of X-ray inside the cloud is calculated using optical depth defined in Equation (3). For the extinction of UV photons, we use the empirical relationship

$$\frac{A_V}{N_{\text{H}}} = 5.3 \times 10^{-22} \text{ mag cm}^2 \text{ H}^{-1} \quad (7)$$

which is caused mainly by dust (Draine 2011). For reference, the typical visual extinction A_V is 8 mag in a dense molecular cloud and could increase to 15 mag in dense cores (Tielens 2005). In our fiducial model, we set $N_{\text{H}} = 10^{22.5} \text{ cm}^{-2}$ and the corresponding A_V is 16.8. We also experiment with $N_{\text{H}} = 10^{22}$ and 10^{23} cm^{-2} for comparison and the results are shown in §4.3.

We also note that in our fiducial model the initial chemical abundance is out of equilibrium, in the sense that without X-ray irradiation the abundance would still evolve relatively quickly, on a timescale of $10^6 - 10^7$ years. Nevertheless, we choose this initial condition because it agrees better with the observed abundance in several molecular clouds (e.g. Wakelam & Herbst 2008; Quan & Herbst 2007). For old molecular clouds ($\sim 10^7$ years), the chemical abundance could significantly deviate from our initial condition. To account for this possibility, we run additional simulations in which we evolve our network for 10^7 years before we turn on the X-ray irradiation. The results are presented in §4.4.

4. Results

4.1. Fiducial Model

In our fiducial model, the Eddington ratio of the AGN is $\eta = 1$. The molecular cloud is at a Galactic distance of 4 kpc and has a column density of $N_{\text{H}} = 10^{22.5} \text{ cm}^{-2}$ ($A_V = 16.8$). The results for the chemical evolution are shown in Figures 2 and 3. In general, the abundances of molecules on the dust grain surface are several orders of magnitude higher than their gas-phase counterparts. This is mainly because at low temperatures (~ 10 K)

molecules stay on the surface of dust grains, and the grain surface acts as a reaction container and a catalyst leading to much more efficient formation of H_2O , CH_3OH , etc.

For H_2O (Fig. 2), on the grain surface (lower panels), even without X-rays (the black dot-dashed curves) the abundance keeps growing during the first $10^5 - 10^6$ years and afterwards saturates. The increase is caused mainly by two surface reactions, (i) $\text{H}_2 + \text{OH} \longrightarrow \text{H}_2\text{O} + \text{H}$ and (ii) $\text{H} + \text{OH} \longrightarrow \text{H}_2\text{O}$. The first reaction usually predominates because of the high abundance of H_2 , even though the activation energy is high (Hasegawa et al. 1992). The second one has a much lower energy barrier but the rate is limited by the low concentration of atomic H at the grain surface. The saturation of the water surface abundance in the late stage is due to a balance between the photo-evaporation and the formation processes.

If we start X-ray irradiation at the very beginning (green solid curves), the H_2O surface abundance increases faster and in the end slightly exceeds that in the case without X-ray. We find that the first reaction is not significantly affected by the X-ray irradiation, because the H_2 surface abundance only slightly decreases. On the contrary, the second reaction becomes faster because the atomic hydrogen abundance increases significantly due to the X-ray dissociation of H_2 . After we remove the X-ray irradiation at the end of 10^6 years (green dashed curve), the surface abundance of H_2O stays more or less constant. The value is slightly lower than that in the case of X-ray irradiation because atomic H quickly recombine to form H_2 , thus the rate of the second reaction drops.

For the gas phase (the upper panels of Fig. 2), when there is no X-ray, the abundance of H_2O first increases until a plateau is reached around the time of $10^4 - 10^5$ years. During this period, ionization leads to the formation of H_3^+ , which is a highly reactive species that can quickly produce OH^+ , H_2O^+ , and H_3O^+ (Krolik & Kallman 1983). Gaseous water is synthesized mainly by the recombination of H_3O^+ with electrons. Around the time of 10^6 years, the abundance of gas H_2O starts to decrease because the materials such as OH^+ , H_2O^+ , and H_3O^+ run out following the exhaustion of O, so that the formation of H_2O slows down. The final gaseous abundance is limited mainly by the interaction with atomic cations, such as Si^+ through the ion-neutral reaction $\text{Si}^+ + \text{H}_2\text{O} \longrightarrow \text{HSiO}^+ + \text{H}$.

When X-ray irradiation is turned on, the behavior of the water abundance in the gas phase is similar to that on the grain surface. However, both the rise and fall of the H_2O abundance are more prominent, which leads to

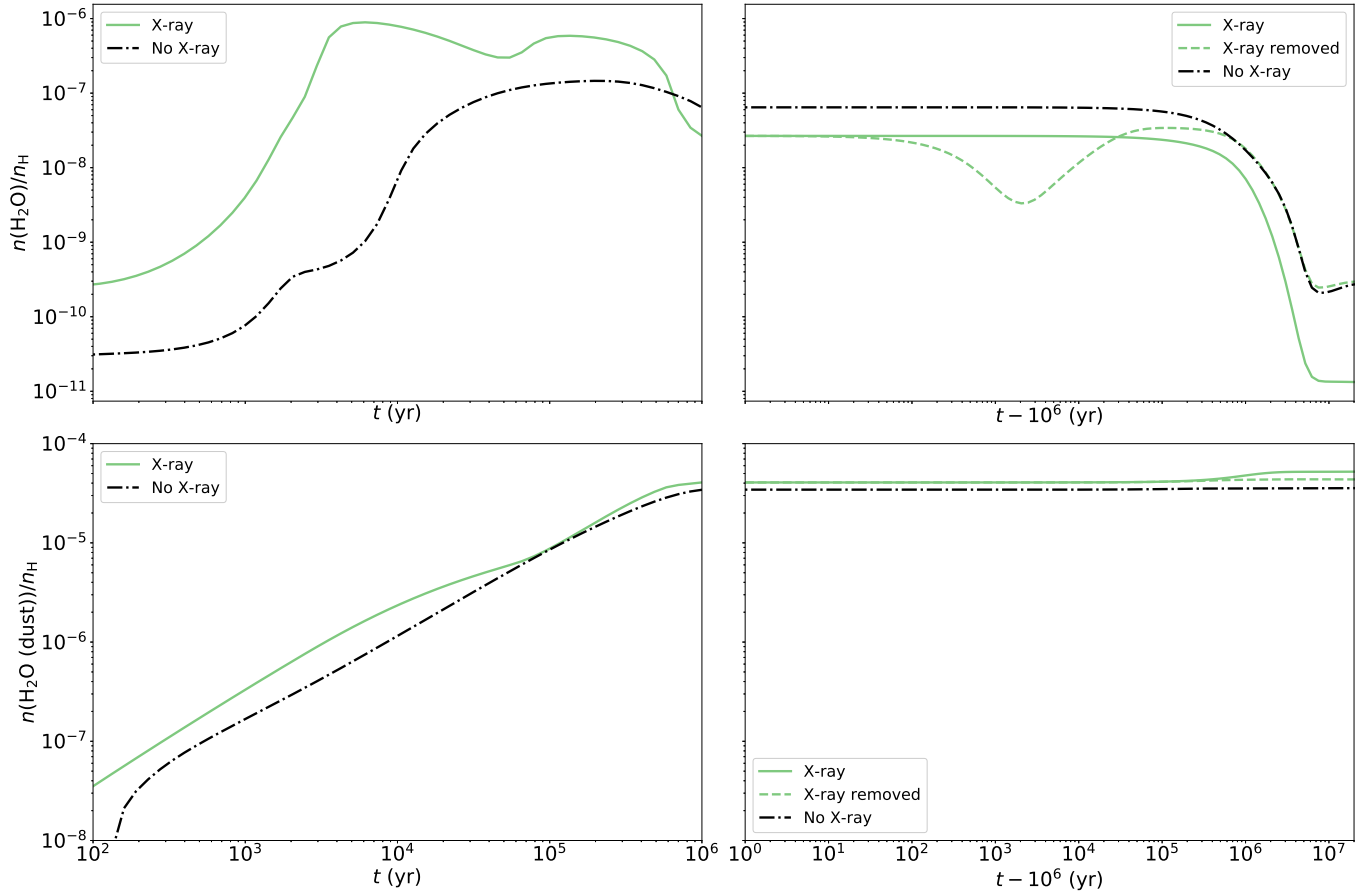


Figure 2. Abundances of H_2O in a molecular cloud 4 kpc away from the galactic center and with a hydrogen column density of $N_{\text{H}} = 10^{22.5} \text{ cm}^{-2}$. The upper panels show the abundance of H_2O in the gas phase and the lower ones show that at the grain surface. The left panels show the first 10^6 years of the chemical evolution and the right ones show the later 10^7 years. The green solid curves correspond to the model in which the AGN persists, while the green dashed ones correspond to the situation where the AGN is turned off after 10^6 years. For comparison, the results when there is no AGN irradiation is shown as the black dot-dashed curves.

a higher plateau around 3×10^5 yr and a lower abundance at about $\gtrsim 10^6$ yr. The sharper evolution is caused by the higher cation density during the X-ray ionization, such as H_3^+ , OH^+ , H_2O^+ , during the early formation stage of H_2O , as well as the higher abundance of Si^+ during the later stage of H_2O destruction. After we remove the X-rays, the abundance of H_2O first decreases but within about 10^5 years recovers the value which is seen in the case of no X-ray irradiation. The recovery is caused by the dissociative recombination, $\text{H}_3\text{O}^+ + e^- \rightarrow \text{H}_2\text{O} + \text{H}$, as well as the photo-evaporation from the grain surface.

For CH_3OH , the evolution of the abundance after the first 10^6 yr is shown in the two upper panels of Figure 3. At the grain surface (right panel), when there is no X-ray irradiation, the abundance is almost constant over 10^7 years of evolution. The dominant synthesis process is hydrogenation, via $\text{CO} \rightarrow \text{HOC} \rightarrow \text{CHOH} \rightarrow \text{CH}_2\text{OH} \rightarrow \text{CH}_3\text{OH}$. When X-ray irradi-

ation is turned on, the abundance of CH_3OH becomes more than two orders of magnitude higher. The increase is caused by a faster hydrogenation process, as the result of a larger atomic-hydrogen abundance due to the X-ray disassociation. Even after we remove the X-ray, the CH_3OH surface abundance stays nearly the same. This is because in our model there is no chemical reaction at the grain surface for CH_3OH destruction (also see Hasegawa et al. 1992) and also the photo-evaporation of CH_3OH is inefficient.

In the gas phase (upper-left panel), without X-ray irradiation, the abundance of CH_3OH stays constant for about 10^6 years and afterwards slightly declines. Gaseous CH_3OH mainly comes from the grain surface, and the later decline is caused by the reactions with cations, e.g., $\text{CH}_3\text{OH} + \text{He}^+ \rightarrow \text{OH} + \text{CH}_3 + \text{He}$ / $\text{OH} + \text{CH}_3^+ + \text{He}$. With X-rays and for the particular Galactic distance of our choice, i.e., 4 kpc, the abundance of CH_3OH increases by about one order of

magnitude relative to that in the case without X-rays. The increase is closely related to the enhancement of the CH_3OH abundance on dust grains. After we remove the X-rays, the abundance increases even more because cations recombine and the destruction of CH_3OH slows down.

For H_2CO , the results are shown in the lower two panels of Figure 3. Unlike CH_3OH which forms only at the grain surface, H_2CO can form both on the surface of grains, mainly through hydrogenation $\text{CO} \longrightarrow \text{HCO} \longrightarrow \text{H}_2\text{CO}$, and in gas phase, via $\text{CH}_3 + \text{O} \longrightarrow \text{H}_2\text{CO} + \text{H}$. Moreover, There is also one pathway for H_2CO on the grain surface to dissociate, $\text{H}_2\text{CO} + \text{H} \longrightarrow \text{HCO} + \text{H}_2$. The O atom can then be transferred to species like CO_2 through reaction $\text{O} + \text{HCO} \longrightarrow \text{CO}_2 + \text{H}$. Although the activation energy of this dissociation is high, the reaction rate is still orders of magnitude higher than photo-evaporation.

With these differences in mind, we can understand the behavior of H_2CO at the grain surface (lower-right panel). During the X-ray irradiation, the formation rate is first enhanced due to a higher hydrogenation rate. In the last several million years of our simulation the abundance of H_2CO significantly decreases, because the disassociation process becomes important and O atoms are slowly transferred to species like CO_2 . After we remove the X-ray irradiation, the decrease of the surface abundance of H_2CO becomes slower because the surface abundance of H falls substantially. Because the formation (hydrogenation) of H_2CO is also proportional to the surface abundance of H, we do not see an increase of H_2CO after we remove the X-ray irradiation.

In the gas (lower-left panel), even without X-rays, the abundance of H_2CO drops by almost four orders of magnitude by the end of the $10^6 - 10^7$ years of evolution. The drop is mainly caused by the exhaustion of CH_3 and O, so that the rate of the reaction $\text{CH}_3 + \text{O} \longrightarrow \text{H}_2\text{CO} + \text{H}$ significantly decrease by the end of our simulation. With X-rays, the abundance decreases relative to that in the case without X-ray irradiation, by a factor of a few. The drop is due to the higher abundance of cations. In this case, the destructive reactions, such as $\text{H}_2\text{CO} + \text{S}^+ \longrightarrow \text{HCO}^+ + \text{HS}$, become more efficient. When we remove the X-rays, the H_2CO abundance first recovers the value in the case of no X-ray irradiation and in about 10^6 years significantly decreases due to the exhaustion of CH_3 . Finally, the abundance balances at a value which is higher than that in the no-X-ray case, because more CH_3 has been produced during the episode of X-ray irradiation.

For completeness, we show in the Appendix [Appendix A](#) the evolution of the other species that are

often detected in molecular clouds. In general, we also find that their abundances with and without X-rays are different.

4.2. Distribution in the Galactic Disk

Since the X-ray flux decreases with increasing distance from the Galactic Center, we also explore the chemical evolution at different Galactic distances. The results are shown in Figure 4, where the column density of each cloud is still set to $N_{\text{H}} = 10^{22.5} \text{ cm}^{-2}$.

On the grain surface (right panels), when there is X-ray irradiation (solid curves), the abundance of H_2O keeps increasing as the Galactic distance decreases. The increase is caused by the higher abundance of atomic hydrogen as the ionization flux intensifies. For CH_3OH and H_2CO , however, the surface abundance maximizes at a Galactic distance of 4 – 8 kpc, and further increasing or decreasing the distance would both lead to a lower abundance. The location where these two abundances peak is determined by two competing processes. On one hand, an important precursor of both species, CO, can be destroyed by X-rays and hence cannot exist too close to the Galactic Center when the AGN is on. On the other, the abundance of H increases towards the AGN due to X-ray disassociation. These two processes balance at about 4 – 8 kpc and produce the highest abundance of CH_3OH and H_2CO there.

To understand the behavior of H_2O , CH_3OH , and H_2CO after we turn off the X-ray irradiation (dashed lines), we should first understand the evolution of H_2 and CO. The major difference between the two species is that while the H_2 abundance is lowered by several percents during the X-ray irradiation, the abundance of CO could be lowered by orders of magnitude depending on the Galactic distance. Therefore, after we turn off the X-rays, the abundance of H_2 only slightly increases in percentage, due to recombination, and recovers the equilibrium in the case of no X-rays, but the abundance of CO increases more drastically. The difference in the recovery rate causes the different behavior of H_2O versus CH_3OH and H_2CO at the grain surface. We can see that after we turn off X-rays, the surface abundance of H_2O increases slightly, because there is slightly more H_2 for the reaction $\text{H}_2 + \text{OH} \longrightarrow \text{H}_2\text{O} + \text{H}$. For CH_3OH and H_2CO , however, there is a lot more CO produced within a short period of time, especially at small Galactic distances. For example, at 1 kpc the abundances of CH_3OH and H_2CO rise by orders of magnitude after the X-ray irradiation is turned off. One interesting result, which is shared by all the three molecular species (H_2O , CH_3OH , and H_2CO) and at all the simulated Galactic distances, is that the final surface abundance after we

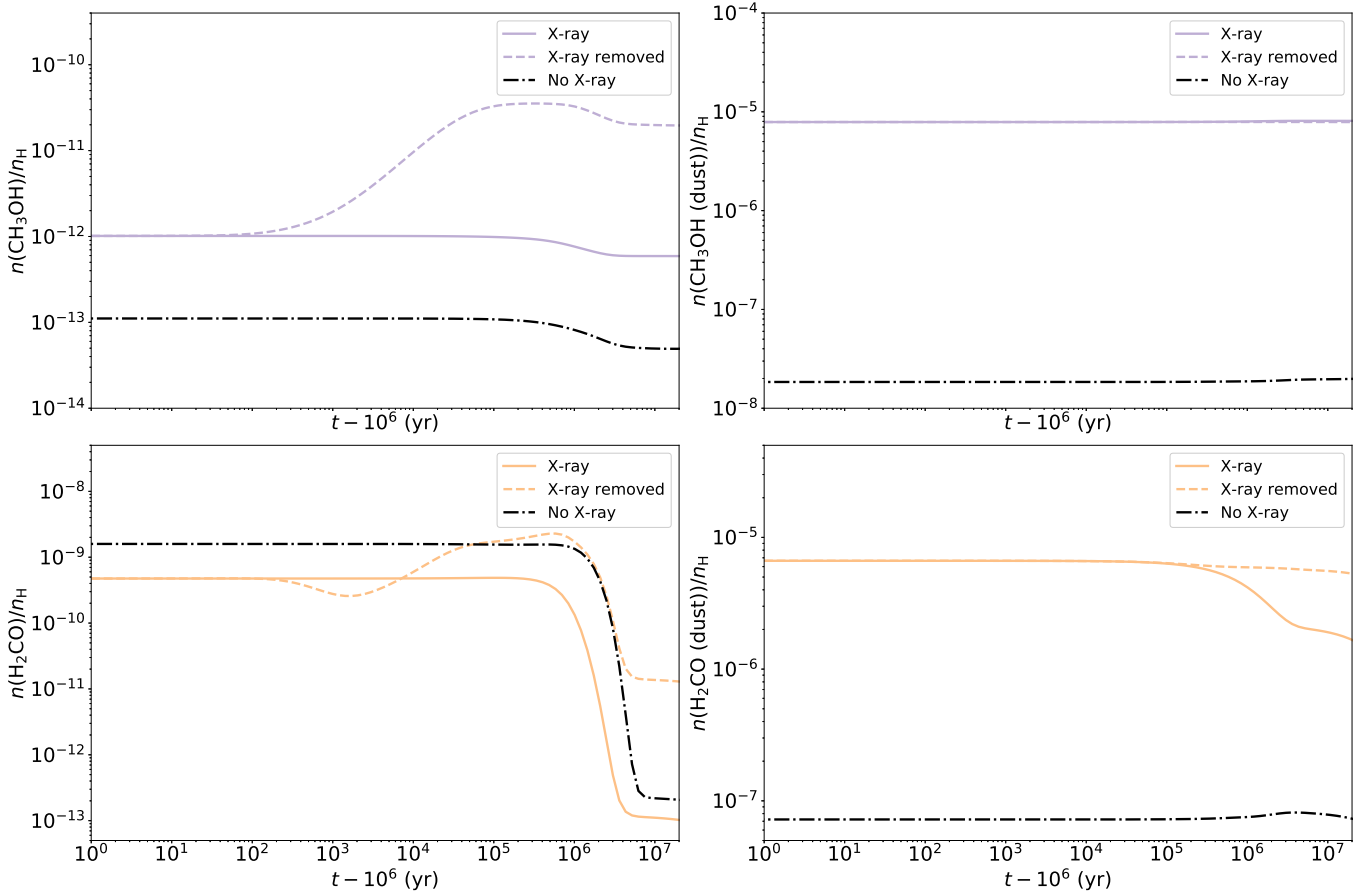


Figure 3. Evolution of the abundances of CH_3OH (upper) and H_2CO (lower) in the gas phase (left) and on the grain surface (right). The line styles have the same meanings as in Fig. 2.

remove X-rays is higher than the abundance in the case without X-ray irradiation.

In the gas phase (left panels), the behavior of H_2O , CH_3OH , and H_2CO also depends on the Galactic distance. For H_2O , the X-ray irradiation in general suppresses the abundance within a timescale of 10^7 years, because, as we have explained in §4.1, destructive cations form in large amount but water formation on the grain surface is relatively inefficient. Moreover, the final abundance decreases with decreasing distance, because the X-ray flux is higher at smaller distance. For CH_3OH and H_2CO , destructive cations also form due to the X-ray irradiation. That is why at small Galactic distances such as 1 and 2 kpc, the abundances of CH_3OH and H_2CO are suppressed when the AGN is on. However, at large distances such as 4 and 8 kpc, the abundances are not significantly suppressed and could even exceed those in the cases without X-rays. The reason is that at these distances the X-ray flux is not as strong so that CH_3OH and H_2CO form very fast on the grain surface, which, through photo-evaporation, could also enrich the gas.

After we turn off the X-ray irradiation, the gaseous abundances of H_2O , CH_3OH , and H_2CO all increase within a timescale of 10^7 years, regardless of the Galactic distance. The cause is mainly the recombination of cations, which in turn lowers the destruction rate. Photo-evaporation also contributes considerably. Even for H_2O , whose gaseous concentration is not as sensitive to the surface abundance, photo-evaporation enriches the gas species significantly after $\sim 5 \times 10^6$ years, when the dissociative recombination has significantly slowed down. We find that at all distances, after we remove the X-rays, the final abundances of gaseous H_2O , CH_3OH , and H_2CO exceed those in the case without an AGN.

These results suggest that a relatively short episode (10^6 years) of X-ray irradiation could indeed, in the following 10^7 years, leave an imprint in the molecular abundances throughout the MW.

4.3. Distribution Inside Molecular Cloud

To understand the distribution of H_2O , CH_3OH , and H_2CO as a function of the depth inside a molecular cloud, we compute the chemical evolution assuming dif-

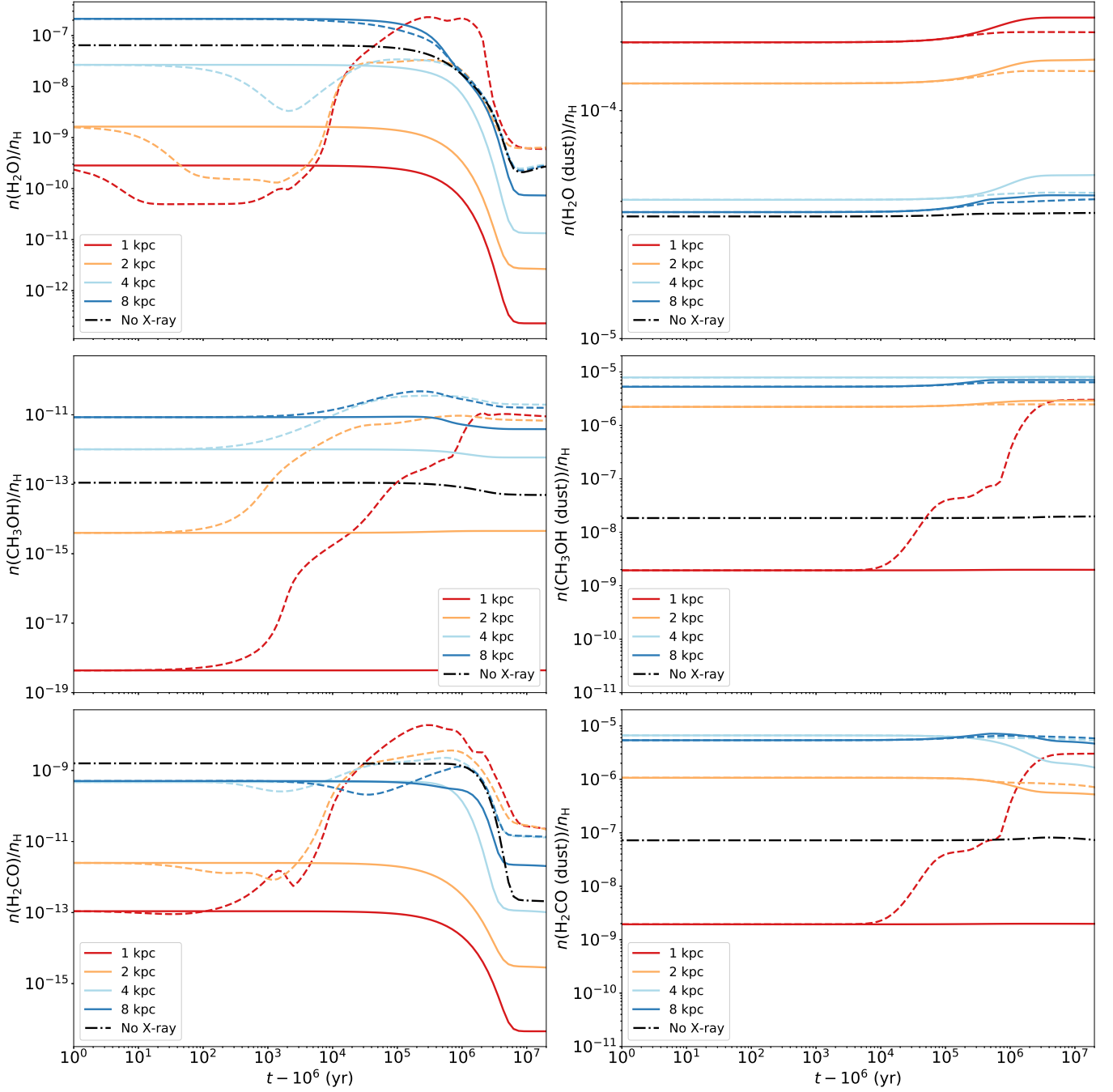


Figure 4. Evolution of the abundances of H_2O , CH_3OH , and H_2CO (from top to bottom) inside the molecular clouds at different Galactic distances (1, 2, 4, and 8 kpc). The left panels show the abundances in the gas phase and the right ones show the surface abundances. The lines styles have the same meanings as in in Fig. 2.

ferent column densities (N_{H}) for the cloud. The results are shown in Figure 5. In these calculations, the Galactic distance of the cloud is fixed at 4 kpc.

We find that when the column density is high, i.e., $N_{\text{H}} = 10^{23} \text{cm}^{-2}$ (or equivalently $A_V = 53$), the abundances (see the blue curves) are slightly, but systematically lower than those in the fiducial model. This trend can be seen both in the gas phase and on the grain sur-

face. The main cause of this systematic change is the lower UV flux due to higher extinction. The hard X-ray flux from the AGN is only slightly attenuated inside the molecular cloud, and hence when we turn on and off the AGN the evolution of the three species is similar to the evolution in our fiducial model.

In low-extinction regions ($N_{\text{H}} = 10^{22} \text{cm}^{-2}$, $A_V = 5.3$), the surface abundances (right panels)

are more significantly affected by the rise of the UV irradiation. Even when there is no X-ray radiation (dotted curves), the H_2O abundance is lower than that in the fiducial case by one order of magnitude. On the contrary, the surface abundances of H_2CO and CH_3OH are higher than those in the fiducial model. This result is caused by two competing processes. On one hand, surface species evaporate more rapidly in the presence of a higher UV flux. On the other, the higher density of H due to UV ionization/dissociation enhances the rate of hydrogenation. Since the synthesis of H_2O uses mainly H_2 , not H, a higher UV flux would increase the evaporation rate more than the hydrogenation one, causing the surface abundance of water to decrease. For CH_3OH and H_2CO , the hydrogenation rate is relatively higher than the evaporation rate, so that the surface abundances increase when the UV flux becomes higher.

If we turn on X-rays, the surface abundances of all the three species increase (compare the red-dotted and the red-solid curves), because of an enhancement of the H density on the grain surface. However, compared to those in the high-extinction regions (blue solid curves), the surface abundances in the low-extinction regions is reduced, because of a higher evaporation rate induced by X-rays in the latter case. After we remove the X-ray irradiation, within $\sim 10^6$ years the abundances recover the values in the case of no X-rays. The quick recovery is closely correlated with the high reaction and evaporation rate in the low-extinction regions.

In the gas phase of the low-extinction regions (red curves in the left panels), the abundances of H_2O , CH_3OH , and H_2CO without X-rays are much higher than those in the high-extinction ones. After we turn on the X-ray irradiation, the abundances become lower, but are still higher than those in the high-extinction regions. The high abundances in the gas are caused mainly by the high photo-evaporation rate on the grain surface. After we turn off X-rays, the gas abundances quickly recover the values in the no-X-ray case, and hence the imprint of the X-rays disappears within about 10^6 years.

4.4. Age of Molecular Cloud

To see the response of a more evolved molecular cloud to the X-rays from the AGN, we run our chemical-reaction network without X-rays for 10^7 years and take the resulting chemical abundances as our new initial condition for the later simulations. The other parameters are the same as in the fiducial model. The results are presented in Figure 6. We see that the abundances in the case without X-rays no longer significantly vary with time, both in the gas and on the grain surface, suggest-

ing that the chemical reactions have reached an equilibrium on a timescale of 10^7 years.

If we turn on X-ray irradiation after the 10^7 years of isolated evolution, on the gains surface (right panels) the abundances of H_2O and CH_3OH will increase, as we have seen in the fiducial model, but the abundance of H_2CO decreases. The decrease is caused by the reaction $\text{H}_2\text{CO} + \text{H} \longrightarrow \text{HCO} + \text{H}_2$, which predominates in the current conditions. We notice that the variation of the abundances of CH_3OH and H_2CO after we turn on X-rays is not as prominent as that in a less evolved cloud (see our fiducial model). This difference indicates that a chemically more evolved cloud is more resilient to X-ray irradiation. After we remove the X-rays, the surface abundances return to the values in the case of no X-ray radiation, on a timescale of about 10^7 years.

In the gas phase (left panels), the X-ray irradiation significantly lowers the abundances of all the three molecules. This behavior is different from that in a less-evolved cloud, where the CH_3OH abundance is enhanced by X-rays (see Fig. 3). After we remove the X-rays, the abundances rise more quickly than that in a less-evolved cloud. As a result of the quick rise, a recovery of the equilibrium state for no X-rays is seen at about $10^4 - 10^5$ years. After this time, the imprint of an AGN is lost.

5. Caveats

Besides photo-desorption (see §2.3), X-rays could also excite an electron to a sufficiently high energy so that it escapes from the grain surface (Draine 2011). These photoelectrons from dust grains, in principle, are energetic enough to ionize the gas molecules, but we did not consider them in this work because of the uncertainty in the calculation of their number (Bakes & Tielens 1994; Weingartner & Draine 2001; Weingartner et al. 2006). The following estimation shows that by neglecting these photoelectrons, we could have underestimated the ionization rate of molecular gas by a factor of 2 – 9, and hence underestimated the effect of the AGN on the molecules in the gas phase.

Following the work of Weingartner et al. (2006) who modeled photoelectric emission from the grains exposed to extreme ultraviolet and X-ray radiation, we assume that (i) the typical dust particles are carbonaceous grains with a radius of $0.1\mu\text{m}$ (cross section $\sim 3 \times 10^{-10} \text{cm}^2$), (ii) after each absorption of a hard-X-ray photon ($h\nu > 1 \text{keV}$) the probability of a photoelectron (either primary or secondary) escaping the bulk solid is 0.1 – 1, and (iii) the photoionization cross section of hydrogen atom in ground state is 10^{-23}cm^2 at 1 keV. Moreover, we adopt the previous assumptions of a gas-to-dust ra-

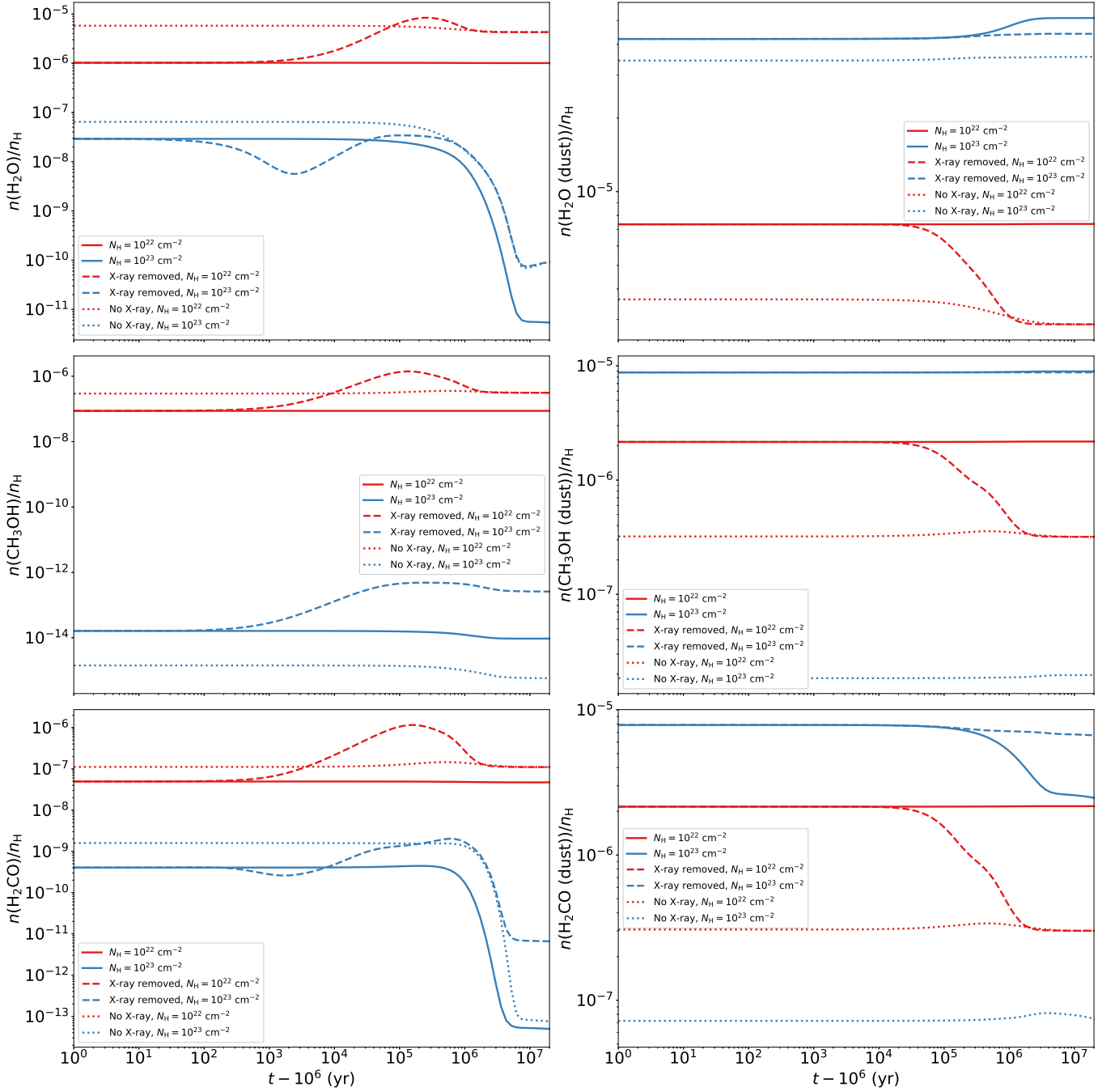


Figure 5. Abundances of H_2O , CH_3OH , and H_2CO (from top to bottom) at different depth of a molecular cloud, located at 4 kpc from the Galactic Center. The depth is proportional to the column density N_{H} . The red curves correspond to a column density of $N_{\text{H}} = 10^{22} \text{ cm}^{-2}$ and the blue ones to 10^{23} cm^{-2} . The left panels show the abundances in the gas phase and the right ones show the abundances on the grain surface.

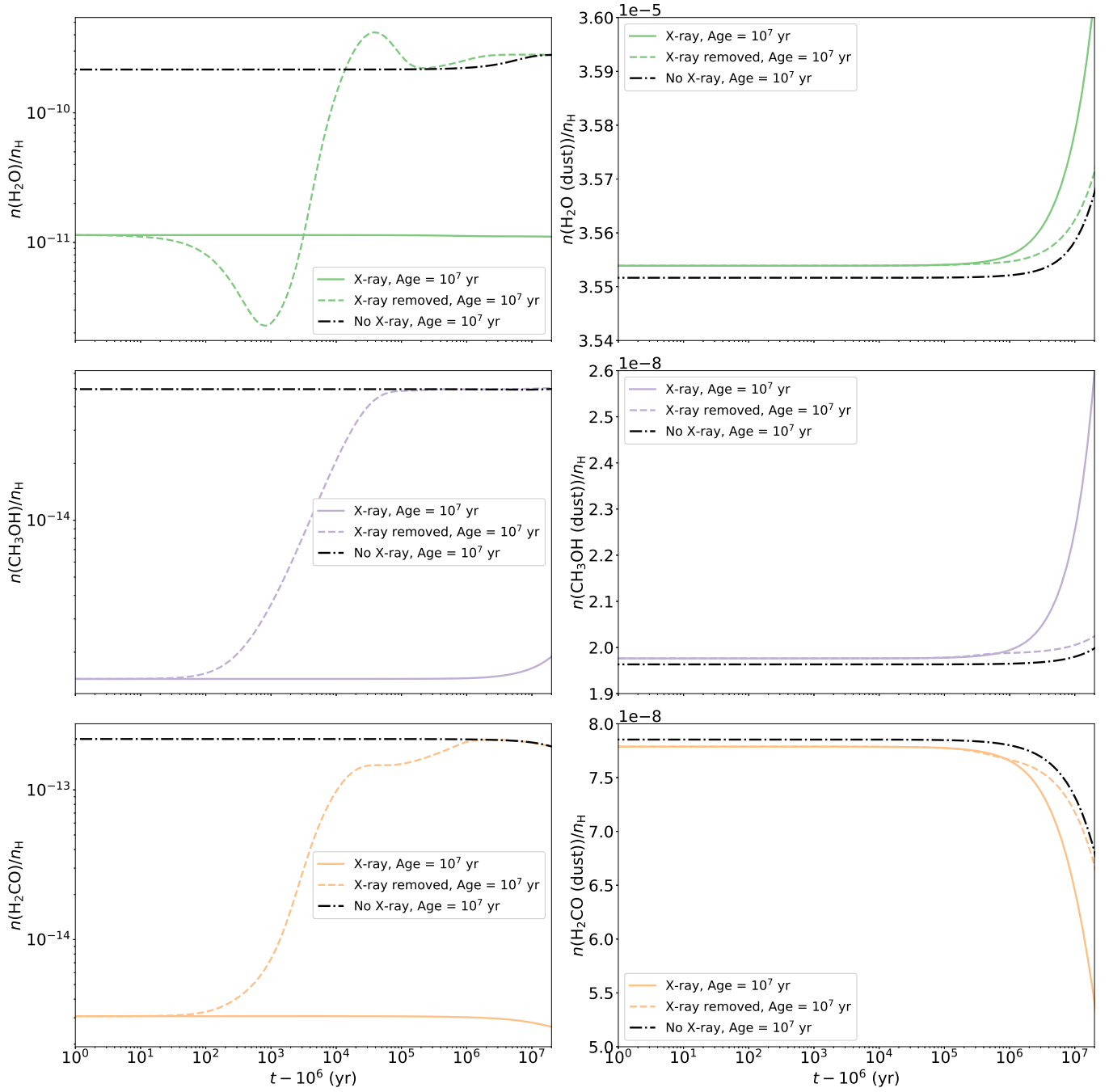


Figure 6. The same as in our fiducial model but the molecular clouds are 10^7 years old in the initial condition of our simulation.

tio of 100 (in mass) and a typical grain density of 3 g/cm^3 . We find that the ratio between the number density of hydrogen atoms and that of carbonaceous grains is 8×10^{11} . Given these numbers, we find that for each X-ray photon of 1 keV the average yield of photoelectrons from dust grains is about 24 – 240. The exact number depends on the sizes of grains which is not well constrained by observations. However, it is about 0.8 – 8 times the yield of photoelectrons from gaseous hydrogen (see §2.1). Therefore, the effect of the photoelectrons from dust grains deserves further investigation.

The loss of photoelectrons would leave the dust grains positively charged. The X-ray induced grain charging has not been modelled in detail until recently (e.g. Ibáñez-Mejía et al. 2019). Charged grains, just like ambient electrons, can affect the temperature of free electrons through Coulomb scattering. They may also react with gaseous anions. However, both free electrons and gaseous anions are rare in the system of our interest. Therefore, we do not consider grain charging in this work.

6. Summary and Conclusion

Motivated by the observational evidence that the SMBH in the Galactic Center could be an AGN several million years ago, we studied the impact of the corresponding X-ray irradiation on the molecular chemistry in the MW. Our main results are summarized as follows.

1. In our fiducial model, a molecular cloud is located at 4 kpc from the Galactic Center and has a column density of $10^{22.5} \text{ cm}^{-2}$. The X-ray irradiation from the AGN could slightly enhance the abundance of H_2O on the surface of dust grains and, at the same time, suppress the water abundance in the gas phase. After the AGN turns off, in the following 10^7 years, the abundance on the grain surfaces remains slightly higher than that in the case without X-rays, while the abundance in the gas phase almost recovers the value of the no-X-ray case.
2. For CH_3OH and H_2CO , our fiducial model shows that the abundances on the grain surface could be enhanced by one to two orders of magnitude during the X-ray irradiation. The enhancement could sustain for about 10^7 years even after the AGN is turned off. In the gas phase, the abundance of CH_3OH is enhanced during the AGN episode by about one order of magnitude, but that of H_2CO is reduced slightly. Interestingly, after we turn off the X-ray irradiation, both abundances rise significantly. Therefore, by the end of the 10^7 years

of simulation, the final gas abundances are higher than the values in the no-X-ray case, by about two orders of magnitude.

3. The exact values of the molecular abundances during and after the AGN episode depend on the distance of the molecular cloud from the Galactic Center. However, there is one feature which appears to be common at different Galactic distances. For a cloud similar to that in our fiducial model, if we irradiate it with X-ray for 10^6 years and then turn off the irradiation for 10^7 years, the final gas and the surface abundances are higher than the case with no X-ray irradiation. The enhancement is the most prominent at small Galactic distances, such as $\lesssim 2$ kpc.
4. After the AGN turns off, the recovery of the molecular abundances is faster in low-extinction regions ($N_H \lesssim 10^{22} \text{ cm}^{-2}$), such as the surface of a molecular cloud or a low-column-density cloud. Therefore, the imprint of a past AGN should be easier to observe in high-column-density regions, e.g., $N_H \gtrsim 10^{22.5} \text{ cm}^{-2}$.
5. Older molecular clouds (e.g. 10^7 years) recover more rapidly after the AGN turns off. Therefore, young molecular clouds are more likely to bear the chemical imprint of a past AGN.

These results suggest that the abundances of molecular species in the MW could be significantly affected and reach a new equilibrium during the past AGN activities of Sgr A*. The chemical imprint of the most recent AGN, which could have occurred several million years ago, may still be found today in those young, high-density molecular clouds residing at relatively small distances from the Galactic Center.

Acknowledgments

This project is under the framework of the Undergraduate Research and Training Program of Peking University and is sponsored by the National Innovation Training Program and School of Physics, Peking University. We thank Jieying Liu for kindly providing us with the AGN spectra of her numerical simulations and Zhu Liu for his help with the UV/X-ray extinction. We also thank Emma Yu and Sarah Dodson-Robinson for a compilation of the relevant literatures. X.C. acknowledges the supported by the NSFC grant No. 11721303. F.D. is supported by One Hundred Person Project of the Chinese Academy of Sciences through grant 2017-089 and by the NSFC grant No. 11873094.

Appendix A Other Important Molecular Species

We also calculated the evolution of several other species that are often observed in molecular clouds, including two molecular ions (HCO^+ , N_2H^+) and six neutral species (NH_3 , CH_4 , CO , HCN , OH , CH_3CN). The abundances on the grain surface and in the gas phase are shown, respectively, in Figures A1 and A2. The Calculation is conducted assuming our fiducial condition.

On the grain surface, the abundances of NH_3 , CH_4 , HCN , OH are enhanced by X-rays, while those of CO and CH_3CN slightly decrease in the presence of X-ray irradiation. In the gas phase, most of these molecular species tend to show lower concentration under X-ray irradiation. When we turn off the AGN, for most species the gas abundances quickly recover, but CH_4 shows a significant excess compared to the abundance in the case without X-rays. HCO^+ and N_2H^+ are temporarily produced in higher efficiency in the first 10^6 years of X-ray irradiation, and then the abundances decrease to values lower than those in the case without X-rays.

References

- Ádámkóvics, M., Glassgold, A. E., & Meijerink, R. 2011, *ApJ*, 736, 143
- Allen, M., & Robinson, G. W. 1977, *ApJ*, 212, 396
- Amaro-Seoane, P., & Chen, X. 2019, *JCAP*, 2019, 056 (Paper I)
- Bakes, E. L. O., & Tielens, A. G. G. M. 1994, *ApJ*, 427, 822
- Balbi, A., & Tombesi, F. 2017, *Scientific Reports*, 7, 16626
- Bland-Hawthorn, J., Maloney, P. R., Sutherland, R. S., & Madsen, G. J. 2013, *ApJ*, 778, 58
- Chen, H., Forbes, J. C., & Loeb, A. 2018, *ApJL*, 855, L1
- Chen, X., & Amaro-Seoane, P. 2015, *CQG*, 32, 064001
- Clarke, J. N. 1981, *Icarus*, 46, 94
- Davies, R., Mark, D., & Sternberg, A. 2012, *A&A*, 537, A133
- Draine, B. T. 1978, *ApJS*, 36, 595
- . 2011, *Physics of the Interstellar and Intergalactic Medium*
- Forbes, J. C., & Loeb, A. 2018, *MNRAS*, 479, 171
- Genzel, R., Eisenhauer, F., & Gillessen, S. 2010, *Reviews of Modern Physics*, 82, 3121
- Gonzalez, G. 2005, *Origins of Life and Evolution of the Biosphere*, 35, 555
- González-Alfonso, E., Fischer, J., Isaak, K., et al. 2010, *A&A*, 518, L43
- Grassi, T., Bovino, S., Schleicher, D. R. G., et al. 2014, *MNRAS*, 439, 2386
- Harada, N., Sakamoto, K., Martín, S., et al. 2018, *ApJ*, 855, 49
- Hasegawa, T. I., & Herbst, E. 1993, *MNRAS*, 261, 83
- Hasegawa, T. I., Herbst, E., & Leung, C. M. 1992, *ApJS*, 82, 167
- Herbst, E., & Klemperer, W. 1973, *ApJ*, 185, 505
- Herbst, E., & van Dishoeck, E. F. 2009, *ARA&A*, 47, 427
- Hopkins, P. F., & Hernquist, L. 2009, *ApJ*, 698, 1550
- Hopkins, P. F., Hernquist, L., Cox, T. J., et al. 2006, *ApJS*, 163, 1
- Ibáñez-Mejía, J. C., Walch, S., Ivlev, A. V., et al. 2019, *MNRAS*, 485, 1220
- Imanishi, M., & Nakanishi, K. 2014, *AJ*, 148, 9
- Jiménez-Escobar, A., Ciaravella, A., Cecchi-Pestellini, C., et al. 2018, *ApJ*, 868, 73
- Kormendy, J., & Ho, L. C. 2013, *ARA&A*, 51, 511
- Krolik, J. H., & Kallman, T. R. 1983, *ApJ*, 267, 610
- Latif, M. A., Bovino, S., Grassi, T., Schleicher, D. R. G., & Spaans, M. 2015, *MNRAS*, 446, 3163
- Laviolette, P. A. 1987, *Earth Moon and Planets*, 37, 241
- Lepp, S., & Dalgarno, A. 1996, *A&A*, 306, L21
- Lingam, M., Ginsburg, I., & Bialy, S. 2019, *ApJ*, 877, 62
- Liu, J. Y., Qiao, E. L., & Liu, B. F. 2016, *ApJ*, 833, 35
- Maloney, P. R., Hollenbach, D. J., & Tielens, A. G. G. M. 1996, *ApJ*, 466, 561
- McMillan, P. J. 2017, *MNRAS*, 465, 76
- Mezger, P. G., Duschl, W. J., & Zylka, R. 1996, *A&A Rv*, 7, 289
- Nayakshin, S., & Cuadra, J. 2005, *A&A*, 437, 437
- Quan, D., & Herbst, E. 2007, *A&A*, 474, 521
- Shankar, F., Weinberg, D. H., & Miralda-Escudé, J. 2009, *ApJ*, 690, 20
- Shull, J. M., & van Steenberg, M. E. 1985, *ApJ*, 298, 268
- Soltan, A. 1982, *MNRAS*, 200, 115
- Stäuber, P., Doty, S. D., van Dishoeck, E. F., & Benz, A. O. 2005, *A&A*, 440, 949
- Su, M., Slatyer, T. R., & Finkbeiner, D. P. 2010, *ApJ*, 724, 1044
- Takano, S., Nakajima, T., Kohno, K., et al. 2014, *PASJ*, 66, 75
- Tielens, A. G. G. M. 2005, *The Physics and Chemistry of the Interstellar Medium* (Cambridge: Cambridge Univ. Press)
- Usero, A., García-Burillo, S., Fuente, A., Martín-Pintado, J., & Rodríguez-Fernández, N. J. 2004, *A&A*, 419, 897
- Verner, D. A., Ferland, G. J., Korista, K. T., & Yakovlev, D. G. 1996, *ApJ*, 465, 487
- Visser, R., Doty, S. D., & van Dishoeck, E. F. 2011, *A&A*, 534, A132
- Volonteri, M. 2010, *A&A Rv*, 18, 279
- Wakelam, V., & Herbst, E. 2008, *ApJ*, 680, 371

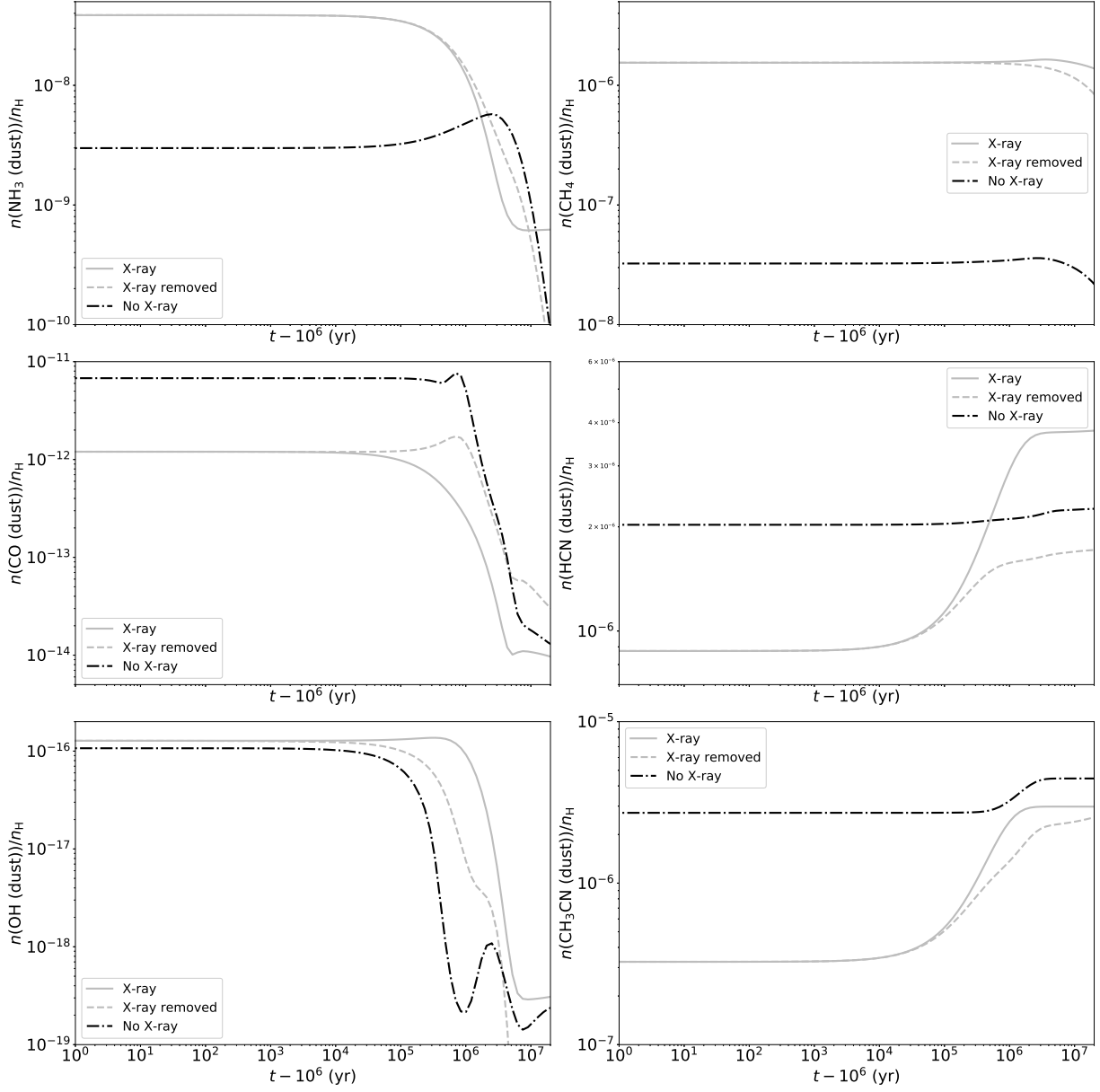


Figure A1. Abundances of NH_3 , CH_4 , CO , HCN , OH , CH_3CN on the grain surface as a function of time in our fiducial model.

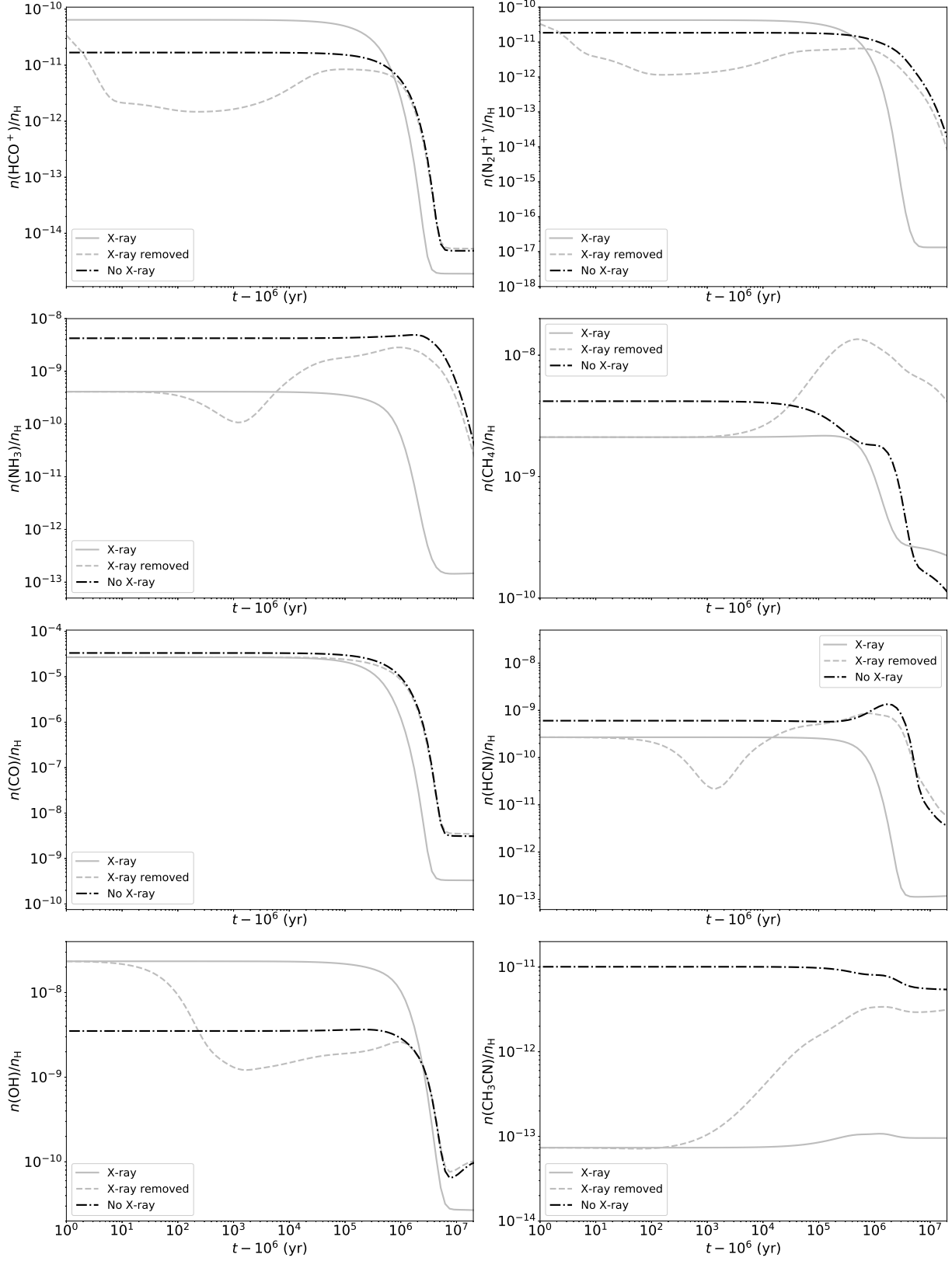


Figure A2. Same as Fig. A1 but for the molecules in the gas phase. Two molecular ions (HCO^+ and N_2H^+) are also included

Wakelam, V., Smith, I. W. M., Herbst, E., et al. 2010,
SSRv, 156, 13

Weingartner, J. C., & Draine, B. T. 2001, ApJS, 134, 263

Weingartner, J. C., Draine, B. T., & Barr, D. K. 2006, ApJ,
645, 1188

Wisłocka, A. M., Kovačević, A. B., & Balbi, A. 2019, A&A,
624, A71